Choice of First Wall Material in the Light Ion Beam Target Development Facility

R.R. Peterson, G.A. Moses, and K.J. Lee

February 1982

UWFDM-456

FUSION TECHNOLOGY INSTITUTE

UNIVERSITY OF WISCONSIN

MADISON WISCONSIN

Choice of First Wall Material in the Light Ion Beam Target Development Facility

R.R. Peterson, G.A. Moses, and K.J. Lee

Fusion Technology Institute
University of Wisconsin
1500 Engineering Drive
Madison, WI 53706

http://fti.neep.wisc.edu

February 1982

UWFDM-456

Choice of First Wall Material in the Light Ion Beam Target Development Facility

R.R. Peterson, K.J. Lee, A. White, R. Engelstad,
E.G. Lovell, G.L. Kulcinski, and G.A. Moses

Fusion Engineering Program
Nuclear Engineering Department
University of Wisconsin
Madison, WI 53706

February 1982

UWFDM-456

Abstract

The choice of material for the first wall of the Light Ion Beam Target Development Facility is discussed. Materials considered are Al 6061, Al 5086, 304 stainless steel, HT-9 (ferritic steel), Ti-6Al-4V, Cu-Be C17200, and Cu-Be C17600. The thermal response, mechanical response and induced radioactivity in first walls made of each of these materials are calculated. Minimum thicknesses of these walls are determined and cost estimates are made for the material requirements for each wall. Finally Al 6061 is suggested as the best choice of first wall material.

I. Introduction

First wall design is a critical part of Inertial Confinement Fusion reactor design[1-4] and is also important to any experimental device where repetitive fusion target explosions are to be contained. An important first wall design feature is the choice of material. Important issues in the choice of first wall material include chemical compatibility with coolants and cavity gases, tritium retention, induced radioactivity, mechanical response to shocks and thermal response to heat fluxes. In this paper, these issues are faced for the first wall design in the Light Ion Beam Target Development Facility (TDF)[5] shown in Fig. 1.

In the TDF, fusion targets yielding approximately 200 MJ of energy would be tested roughly 10^4 times during the lifetime of the facility at the rate of 10 shots/day. The target chamber is a cylinder 3 meters in radius and is filled with 5-50 torr of gas. The target explosion generates a blast wave in the cavity gas that transmits a pulsed heat flux and a shock overpressure to the first wall. These effects have been simulated by the computer code FIRE[6] for various densities of argon with a 0.2% impurity of sodium and of xenon with a 0.5% impurity of cesium. The results of these simulations are shown in Table I where the density is expressed as the pressure the gas would have at room temperature. The maximum overpressure, the arrival time of the mechanical shock at the first wall, the maximum heat flux, its arrival time, and the temperature that an HT-9 wall would attain are all shown in Table I. Since there is some uncertainty about what cavity gas pressure would fill the TDF target chamber, the wall should be designed at this time to withstand the largest possible overpressure and the largest feasible heat flux.

Figure 1

Light Ion Beam Target Development Facility

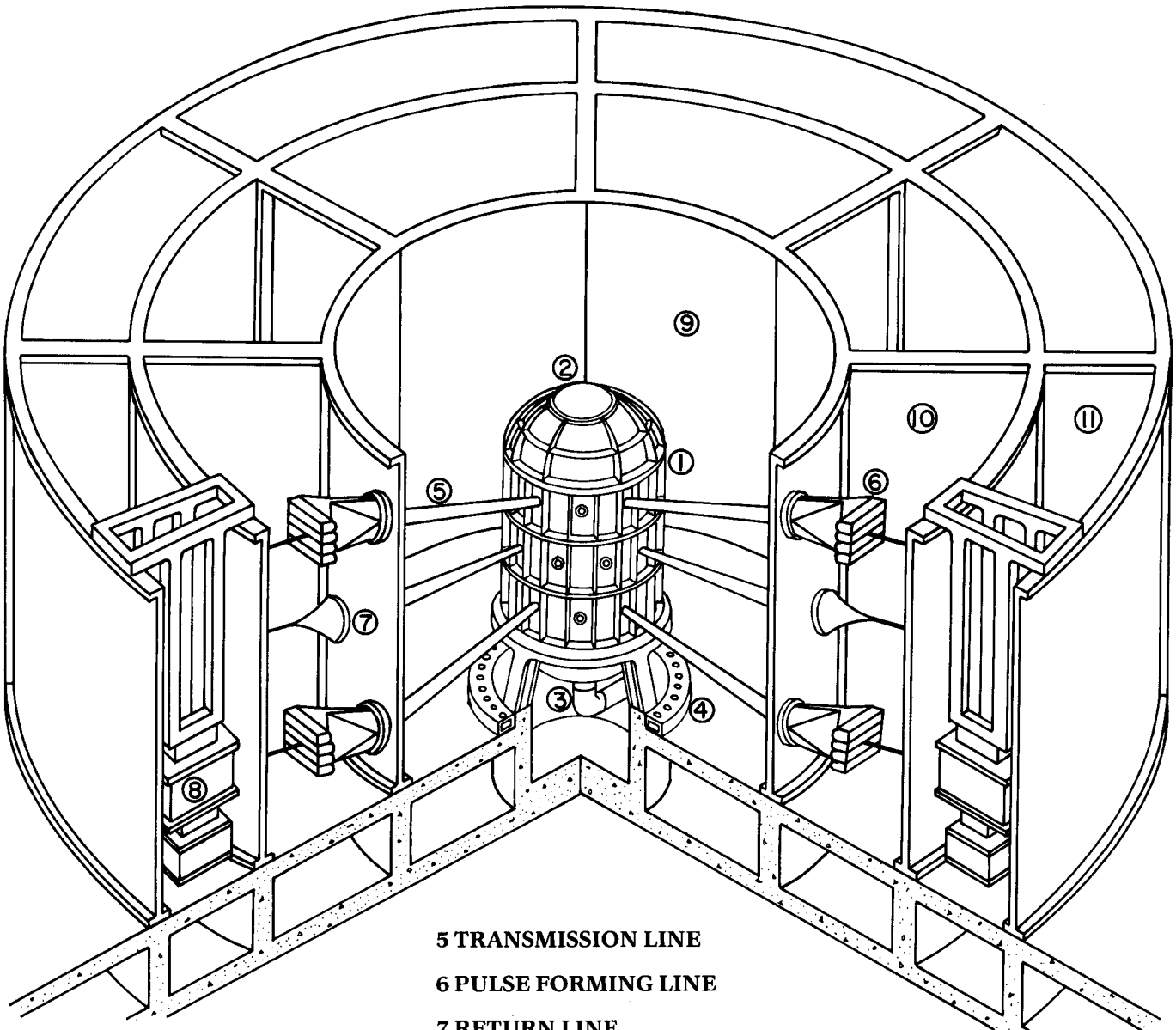

1 TARGET CHAMBER

2 DIAGNOSTIC PORT

3 PURGE LINE

4 AIR BUBBLE PLENUM

5 TRANSMISSION LINE

6 PULSE FORMING LINE

7 RETURN LINE

8 BEAM MARX GENERATOR

9 SHIELDING POOL – WATER

10 PULSE FORMING SECTION – WATER

11 ENERGY STORAGE SECTION – OIL

Table I. Pressure, Heat Flux, and Temperature at First Wall

(200 MJ Explosion, Cavity Radius = 3 m)

Gas (Ambient)	Gas Pressure	Code Version	ΔP_{max} (Overpressure)		Q''_{max} (Heat Flux)		ΔT_{max} (°C) at Wall*
			MPa	Time (msec)	kW/cm^2	Time (msec)	
Argon and 0.2% Sodium	10 Torr	FIRE	0.21	0.31	123	0.184	1244
		X-RAY	0.20	0.33	114	0.183	1203
	20 Torr	FIRE	0.64	0.43	42	0.45	662
		X-RAY	0.61	0.43	42	0.32	675
	50 Torr	FIRE	1.25	0.626	20.5	0.676	294
		X-RAY	1.29	0.613	22.6	0.664	324
	70 Torr	FIRE	1.64	0.67	20.9	0.69	300
Xenon and 0.5% Cesium	5 Torr	X-RAY	0.089	0.136	422	0.136	2901
	10 Torr	FIRE	0.18	0.40	177	0.386	1670
	20 Torr	FIRE	0.69	0.695	92	0.695	809
	50 Torr	FIRE	1.33	1.16	19	1.16	243
	70 Torr	FIRE	1.71	1.32	12.9	1.35	150

*Wall material is HT-9.

Several materials are proposed for the first wall. They are listed in Table II along with some qualitative properties of the materials. Mechanical strength, level of thermal stresses, induced radioactivity and materials costs will be discussed in various sections of the paper. The other properties listed in Table II are fabricability, compatibility with cavity gas, T_2 retention, and compatibility with borated water. Notice that as long as the cavity gas is dry NH_3 or N_2, the only material with any problems is Ti-6Al-4V having a high T_2 retention. If the cavity gas is NH_3, much of the tritium may get bound up in NT_3 and T_2 retention might no longer be a problem. If the cavity gas contains Na or Cs then aluminum is not a good first wall choice.

In Section II, the mechanical and thermal properties of each of these materials is investigated. In Section III we describe mechanical and fatigue response and determine the thickness of each material needed to support the load of the overpressure. In Section IV, the thermal response is investigated and the first wall panel thickness of each material is given. Cost estimates for the first wall materials are made in Section V and the induced radioactivity calculations are described in Section VI. Conclusions and a recommended choice of material are made in Section VII.

II. Thermal and Mechanical Properties

Before any calculations of the first wall mechanical and thermal response can be made, material properties must be identified. The choices of the first wall materials for the TDF cavity are aluminum based alloys (Al 6061 and Al 5086), copper based alloys (Cu-Be C17200 and Cu-Be C17600), titanium alloys (Ti-6Al-4V), and iron based alloys (stainless steel 304 and HT-9). It should be noted that the most important criterion for choosing the candidate materials

Table II. Qualitative Summary of Materials Properties

Metal Alloy	Mech. Strength	Thermal Stress	Fabricability	Unfabricated $\frac{\text{cost}}{\text{unit mass}}$	Induced Radioactivity	Compatibility with Cavity Gas Na/Cs	Compatibility with Cavity Gas N_2	T_2 Retention	Compatibility with Borated H_2O at Room Temperature
Al 6061 Al 5086	Adequate	Very good	Good	Very low	Low	Bad (NaOH dissolves Al)	Good	Good	Good ?
304 SS	Good	Poor	Good	Very low	High	Good	Good	Good	Good
HT-9	Good	Fair	Adequate	Very low	High	Good	Good	Good	Good
Ti-6Al-4V	Adequate	Poor	Adequate	Very high		Good - Oxide layer makes Ti compatible with almost everything	Good - Oxide layer	Bad	Good
Cu-Be	Adequate	Very Good	Fair	Moderate		Okay - NaCl, NaOH	Bad - with moist NH_3 Good - with dry NH_3	Good	Good

is the availability of a qualified metal industry. This criterion is met for all of the candidates.

The thermal (physical) and mechanical properties of the candidate metal alloys are important to the viability of the proposed TDF cavity design. Critical properties include density, heat capacity, thermal conductivity, melting temperature, thermal expansion coefficient, Poisson's ratio, Young's modulus, and tensile yield strength. There is a wide data base for the selected metal alloys with respect to non-fusion environments. Areas such as thermal properties of the candidate metal alloys at room temperature are well known because of their role in aerospace and fission technologies and there is a fair amount of data for moderately elevated temperatures.[7] Most of the data have been obtained from a recently published Metals Handbook[8] and the Structural Alloys Handbook.[9] A recent review of data for HT-9 is found in the "STARFIRE" report.[10] Table III summarizes the data base for the selected metal alloys and contains a quantitative comparison of the seven alloys considered in terms of the thermal and mechanical properties which are the most important to TDF cavity wall design philosophy.

The overall qualitative nature of the thermal properties can be well represented by examining the thermal diffusivity. Aluminum and copper alloys have superior thermal diffusivity compared to that of Ti and Fe based alloys. They allow a much lower temperature gradient at the first wall and will lead eventually to much smaller thermal stresses in the wall. However, their potential disadvantages are connected with their lower melting temperatures. This disadvantage might be corrected by allowing a melting layer at the surfaces facing the incident radiating heat flux. Temperature diffusion calculations indicate that all the candidate metal alloys show much higher maximum

Table III. Thermal and Mechanical Properties of Selected Metal Alloys (Room Temperature)

Metal Alloys	Temper Type	Density (ρ)	Specific Heat (C_p)	Thermal Conductivity (K)	Diffusivity ($K/\rho C_p$)	Melting Point	Thermal Expansion Coefficient (α)	Poisson's Ratio (ν)	Young's Modulus (E)	Yield Strength (σ_y)	$\frac{K(1-\nu)}{\alpha E}$	$\frac{2\sigma_y K(1-\nu)}{\alpha E}$
		g/cm^3	J/g·°K	W/m-°K	cm^2/sec	°C	$10^{-6}/°K$		GPa (KSI)	MPa (KSI)	W/m·MPa	W/m
Al 6061	T6	2.70	0.90	167	0.687	652	23.6	0.33	69 (10,000)	276 (40)	68.7	37920
Al 5086	H34	2.66	0.90	127	0.530	640	23.8	0.33	71 (10,300)	255 (37)	50	25680
304 SS	Annealed	8.0	0.50	16.2	0.0405	1375 ~ 1440	17.2	0.29	193 (28,000)	255 (36.9)	3.4	1750
HT-9		7.75	0.59	29	0.0634	1427 ~ 1482	10.6	0.265	200 (29,000)	442 (64)	10	8870
Ti-6Al-4V	Solution Treated and Aged Bar	4.43	0.67	6.8	0.0222	1660	8.8	0.33	110 (16,000)	1070 (155)	4.7	10030
Cu-Be (C17200)	TB00	8.25	0.42	118	0.340	980	16.7	0.3	128 (18,500)	283 (41)	38.7	21890
Cu-Be (C17600)	TB00	8.75	0.42	230	0.626	1068	16.7	0.3	128 (18,500)	173 (25)	75.5	26050

(Refs.: 1) Metals Handbook, 9th ed., American Society for Metals, Metals Park, Ohio (1979).
2) Structural Alloys Handbook, Battelle's Columbus Laboratories, Columbus, Ohio (1981).
3) Aerospace Structural metals Handbook, Mechanical Properties Data Center, Belfour Stulen, Inc., Traverse City, Michigan (1975, 1981).
4) C.C. Baker et al., "STARFIRE - A Commercial Tokamak Fusion Power Plant Study," Argonne National Laboratory (1980).

temperature differences at the wall than their own melting temperatures. This will be discussed in Section IV.

The mechanical properties of the selected metal alloys are also given in Table III. In terms of mechanical properties, combinations of low thermal expansion coefficients, smaller Young's modulii and high yield (tensile) strengths are desirable. For example, Ti-6Al-4V has a smaller thermal expansion coefficient and larger yield strength than the others. However, it has a much smaller thermal conductivity, which imposes a large thermal stress at the cavity wall as mentioned before. To resolve the paradox of the strongest materials having the worst thermal properties and to qualitatively represent the overall nature of the combined thermal and mechanical properties, the so-called thermal shock parameter is used. This parameter is a measure of the resistance of the metals to thermal stress failure and is defined as

$$P = \frac{2\,\sigma_y K(1 - \nu)}{\alpha E}$$

where: σ_y = yield (tensile) strength

K = thermal conductivity

ν = Poisson's ratio

α = thermal expansion coefficient

E = Young's modulus.

A larger value of P is preferred. It can be seen from Table III that Al and Cu based metal alloys have larger thermal shock parameters compared to that of the Fe and Ti based alloys.

It is well known that most of the metal alloys show wide variations in the thermal and mechanical properties depending on heat treatment, processing

variables and temperatures. Table IV shows the variations of the properties with respect to temper type and temperature. Aluminum based alloys have quite poor values as the temperature increases, while titanium alloys have an increasing value of the thermal shock parameter. Fe based alloys almost remain constant at elevated temperatures. The data base for the copper metal alloys suffers from the lack of related data at high temperatures.

A few important conclusions are drawn from this comparison:

1. The large value of thermal diffusivity for Al and Cu based alloys makes them clearly superior to Fe and Ti based alloys, even though their melting temperatures are relatively lower.
2. Al and Cu based alloys appear to be better choices again with respect to minimizing the thermal stresses due to much higher values of the thermal shock parameter.

III. Mechanical Response of the First Wall

One important constraint on the first wall material and design is that the stresses due to the flexure of wall panels must not exceed either the tensile yield stress or the stress that would lead to fatigue failure during the first wall lifetime. The first wall should last 10^7 flexures if 10^4 target explosions are expected and 10^3 flexures are allowed for each shot. This may be a conservative number but, as is shown in Section IV, it does not lead to excessively thick panels. Since determination of the damping of the flexures is very difficult and depends on the details of the design, it is clearly better to be conservative and choose a large number of flexures per shot. The tensile yield stresses are taken from the values tabulated in Section II. The requirement that the stress remain below the yield stress comes from a desire for the wall to retain its structural integrity. If the

Table IV. Thermal and Mechanical Properties of Selected Metal Alloys

Metal Alloy	Temper Type	Temperature	Thermal Conductivity (K)	Poisson's Ratio ν	Thermal Expansion Coefficient (α)	Young's Modulus (E)	Yield Strength (σ_y)	$\frac{K(1-\nu)}{\alpha E}$	$\frac{2\sigma_y K(1-\nu)}{\alpha E}$
		°C	W/m-°K		10^{-6}/°K	GPa (ksi)	MPa (ksi)	W/m-MPa	W/m
Al 6061	O	25	180	0.33	23.6	69 (10,000)	55 (8)	74	8176
	T4	25	154	0.33	23.6	69 (10,000)	145 (21)	63	18354
	T6	25	167	0.33	23.6	69 (10,000)	276 (40)	69	37920
	T6	300	167	0.33	25.8	38 (5,500)	12.4 (1.8)	114	2837
Al 5086	O	25	127	0.33	23.8	71 (10,300)	117 (17)	50	11800
	H34	25	127	0.33	23.8	71 (10,300)	255 (37)	50	25680
	O	300	127	0.33	25.8	71 (10,300)	29 (4.2)	46	2688

Table IV

Thermal and Mechanical Properties of Selected Metal Alloys - continued

304 SS	Annealed	25	16.2	0.29	17.2	193 (28,000)	255 (36.9)	3.4	1750
	Annealed	500	21.5	0.29	18.2	158 (22,900)	134 (19.4)	5.2	1400
HT-9		25	29	0.265	10.6	200 (29,000)	442 (64)	10	8870
		500	29	0.265	11.8	173 (25,000)	324 (47)	10.5	6796
Ti-6Al-4V	Annealed	25	6.6	0.33	8.8	110 (16,000)	1070 (125)	4.6	7850
	Solution Treated and Aged Bar	25	6.8	0.33	8.8	110 (16,000)	863 (155)	4.7	10030
	Solution Treated and Aged Bar	500	12.0	0.33	10.3	79 (11,500)	621 (90)	9.8	12220

Table IV

Thermal and Mechanical Properties of Selected Metal Alloys - continued

Cu-Be (C17200)	TB00	25	118	0.30	16.7	128 (18,500)	195 ~ 380 (28 ~ 55)	38.7	14950 ~ 29370
	TD01	25	118	0.30	16.7	128 (18,500)	415 ~ 605 (60 ~ 88)	38.7	32040 ~ 46980
	TH04	25	118	0.30	16.7	128 (18,500)	1140~1415 (165~205)	38.7	88110 ~ 109470
Cu-Be (C17600)	TB00	25	230	0.30	16.7	128 (18,500)	140 ~ 205 (20 ~ 30)	75.5	20840 ~ 31260
	H04	25	230	0.30	16.7	128 (18,500)	380 ~ 515 (55 ~ 75)	75.5	57310 ~ 78150
	TH04	25	230	0.30	16.7	128 (18,500)	690 ~ 825 (100~120)	75.7	104200 ~ 125040

wall material is forced to yield repetitively, the lifetime of the panel will be substantially reduced.

The mechanical flexural stresses are calculated for the largest overpressure which could be expected in the TDF cavity gas. This overpressure, which is shown in Fig. 2, was determined by a FIRE code[6] simulation of the response of a 70 torr cavity gas of xenon with a 0.5% impurity of cesium. The greatest reasonable overpressure is used because of the uncertainty in cavity gas response to the target microexplosion. Note that at lower pressures, such as 10 torr, the overpressure is a factor of 10 less. Hence, this is a very conservative choice.

The method of determining the flexural stresses is the same as has been previously reported.[11] This method calculates the dynamic response of the first wall panels by multiplying the static values by a dynamic load factor which is a time-dependent function that includes the effects of material properties and the geometry of the panels. Figures 3 and 4 show the flexural stresses at the inside edge of a panel made of Al 6061 which is 7 cm and 1 cm thick, respectively. In both cases, the dimensions of the panel are 2 meters by 0.47 meters. The panels are assumed to be held fixed on the edges and are solid plates. Notice that the thin panel has a much larger maximum stress and a much lower frequency of oscillation.

The maximum flexural stress has been calculated for several different materials and for plate thicknesses ranging from 1 cm to 7 cm. The dimensions of the panels for all cases are 2 meters by 0.47 meters and they are always solid plates that are held fixed on the edges. In Figs. 5 through 9 the maximum flexural stress has been plotted against plate thickness for Al 6061, 304 stainless steel, HT-9, Ti-6Al-4V, and Cu-Be C17200, respectively. There are

Figure 2 Heat flux and shock overpressure on a 3 meter radius first wall resulting from a 200 MJ microexplosion in a 70 torr gas of xenon with 0.5% cesium.

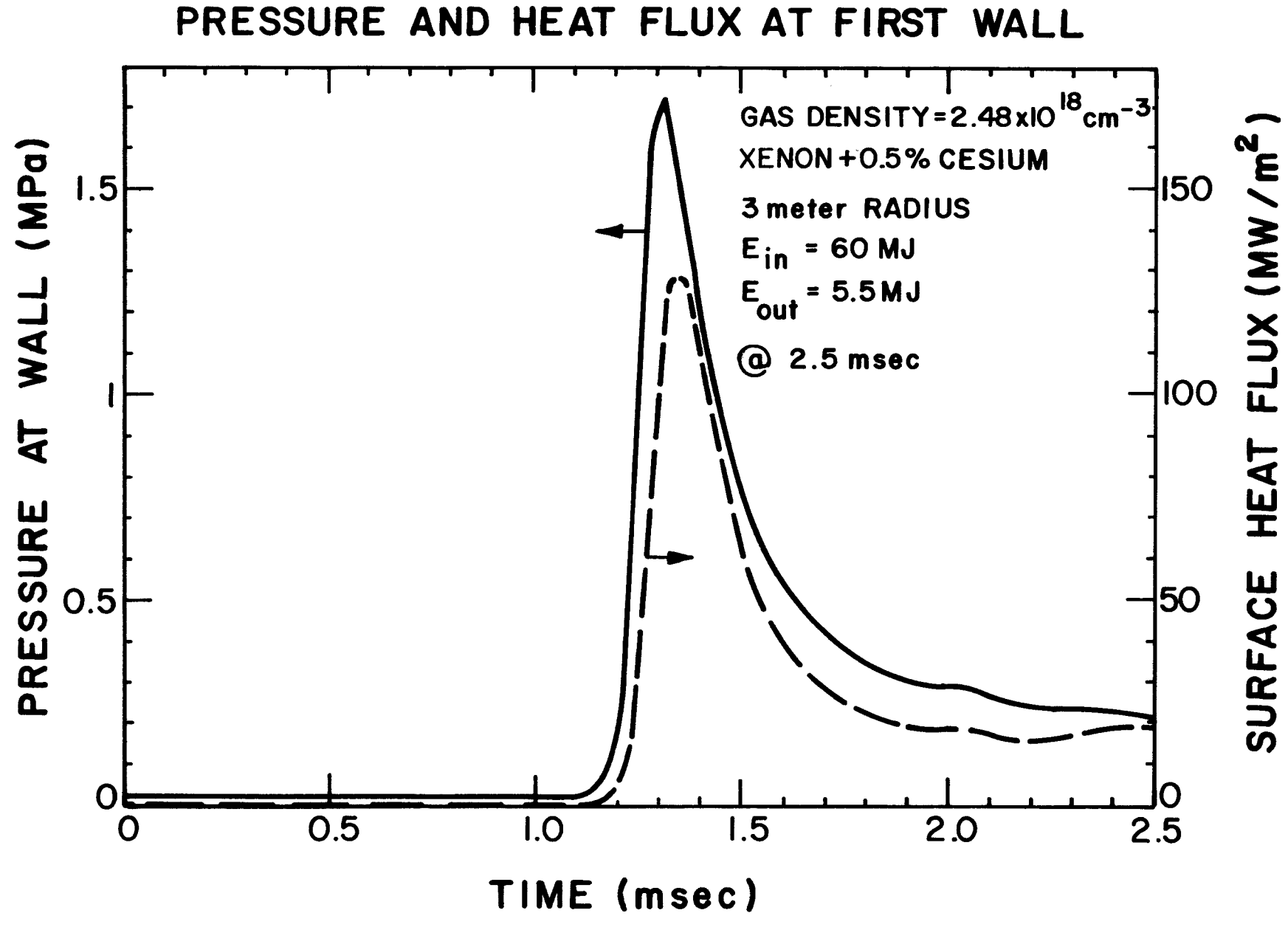

Figure 3 Flexural stress in a 7 cm thick plate of Al 6061 for the pressure pulse shown in Fig. 2.

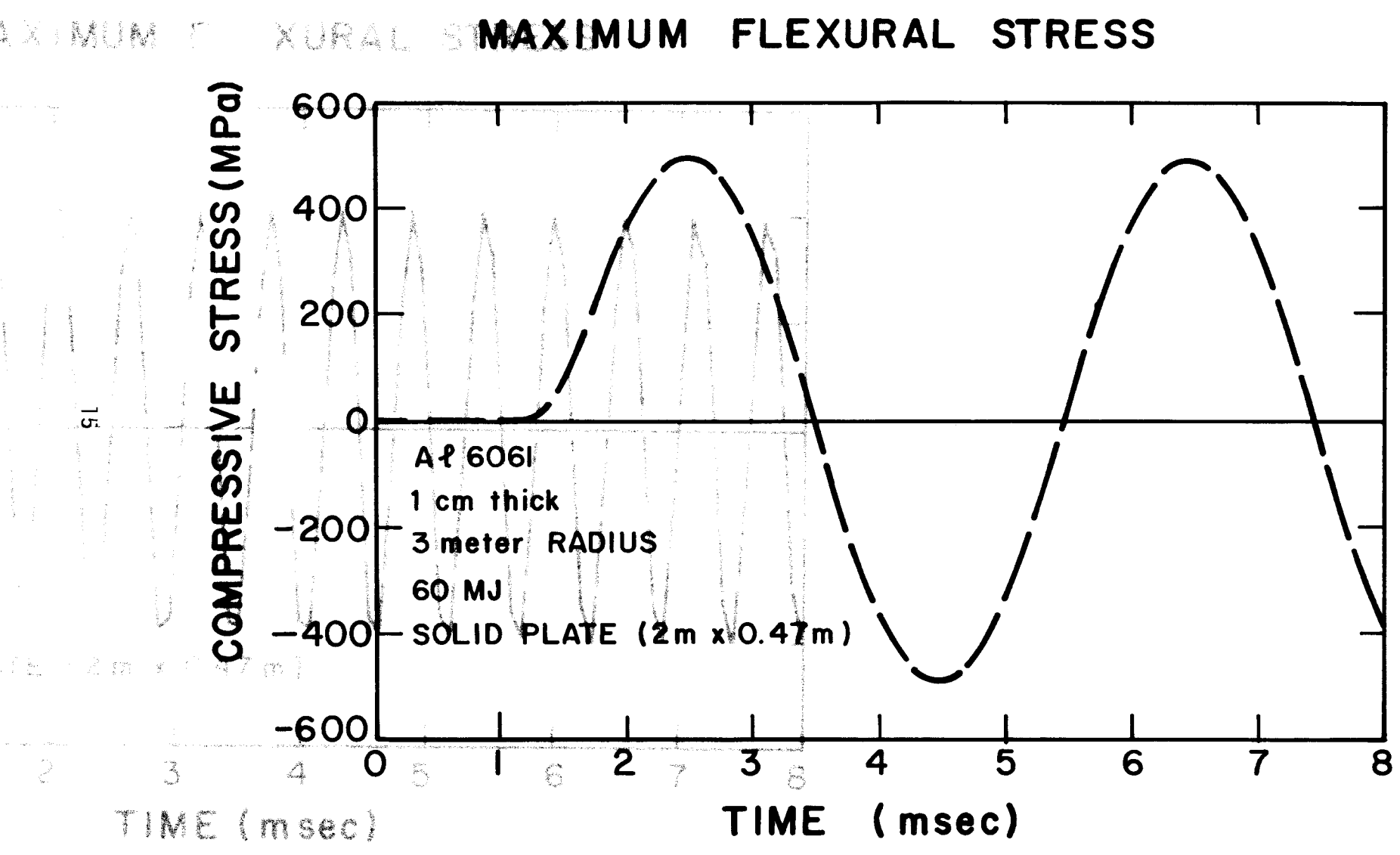

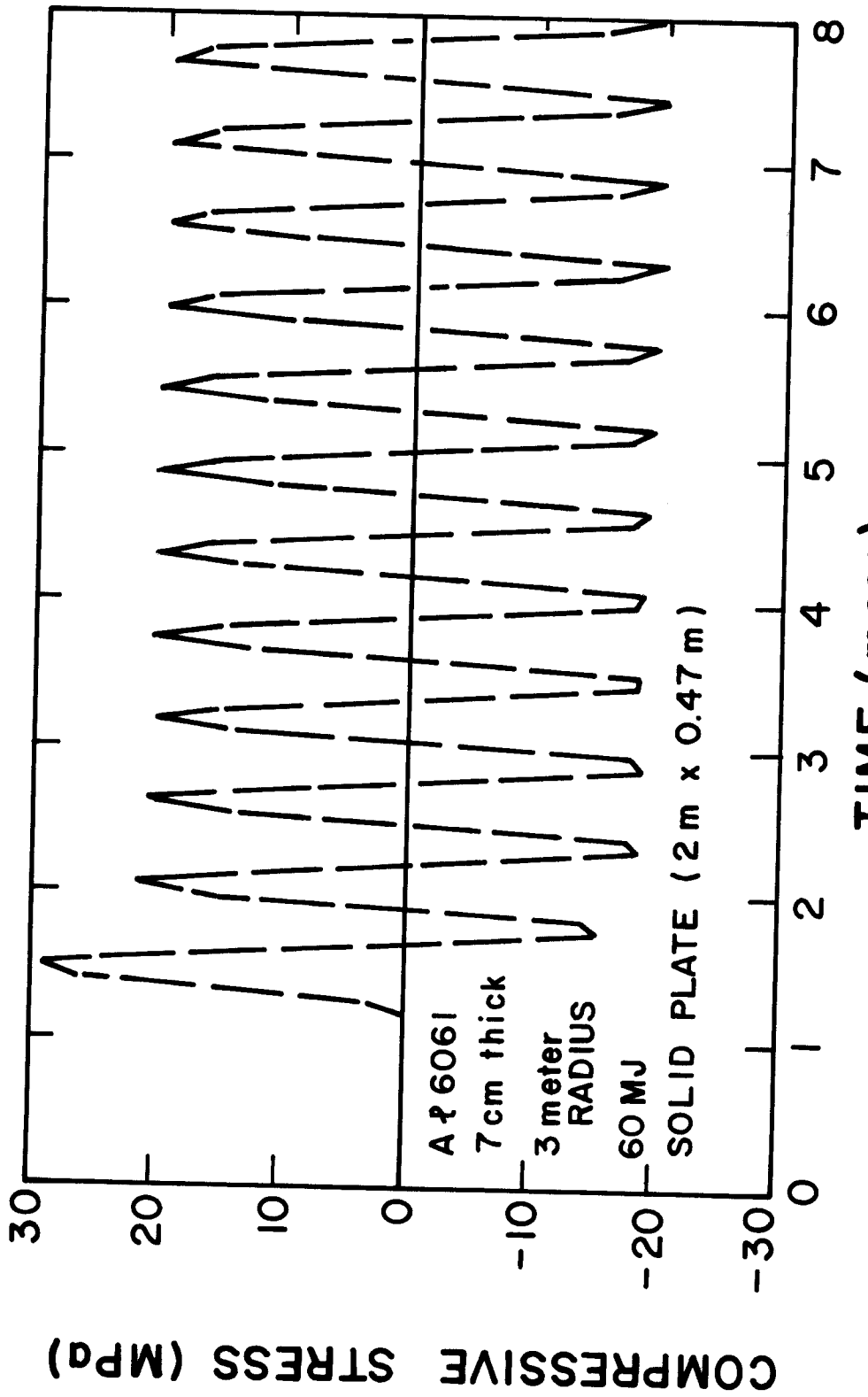

Figure 4 Flexure stress in a 1 cm thick plate of Al 6061 for the pressure pulse shown in Fig. 2.

Fig. 5.

Maximum flexural stresses in a plate of Al 6061 versus plate thickness for the pressure pulse shown in Fig. 2.

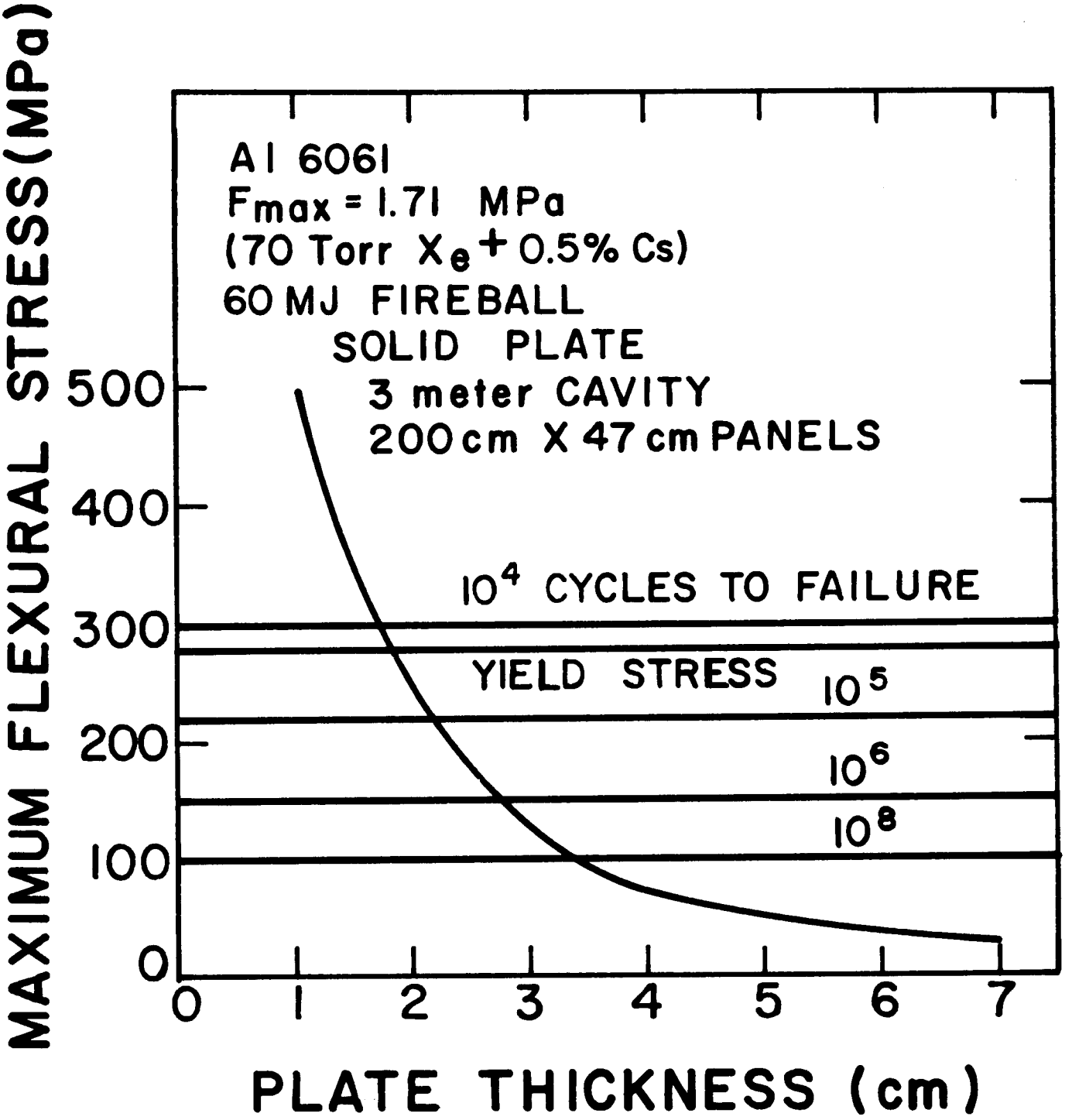

Fig. 6.

Maximum flexural stresses in a plate of 304 stainless steel versus plate thickness for the pressure pulse shown in Fig. 2.

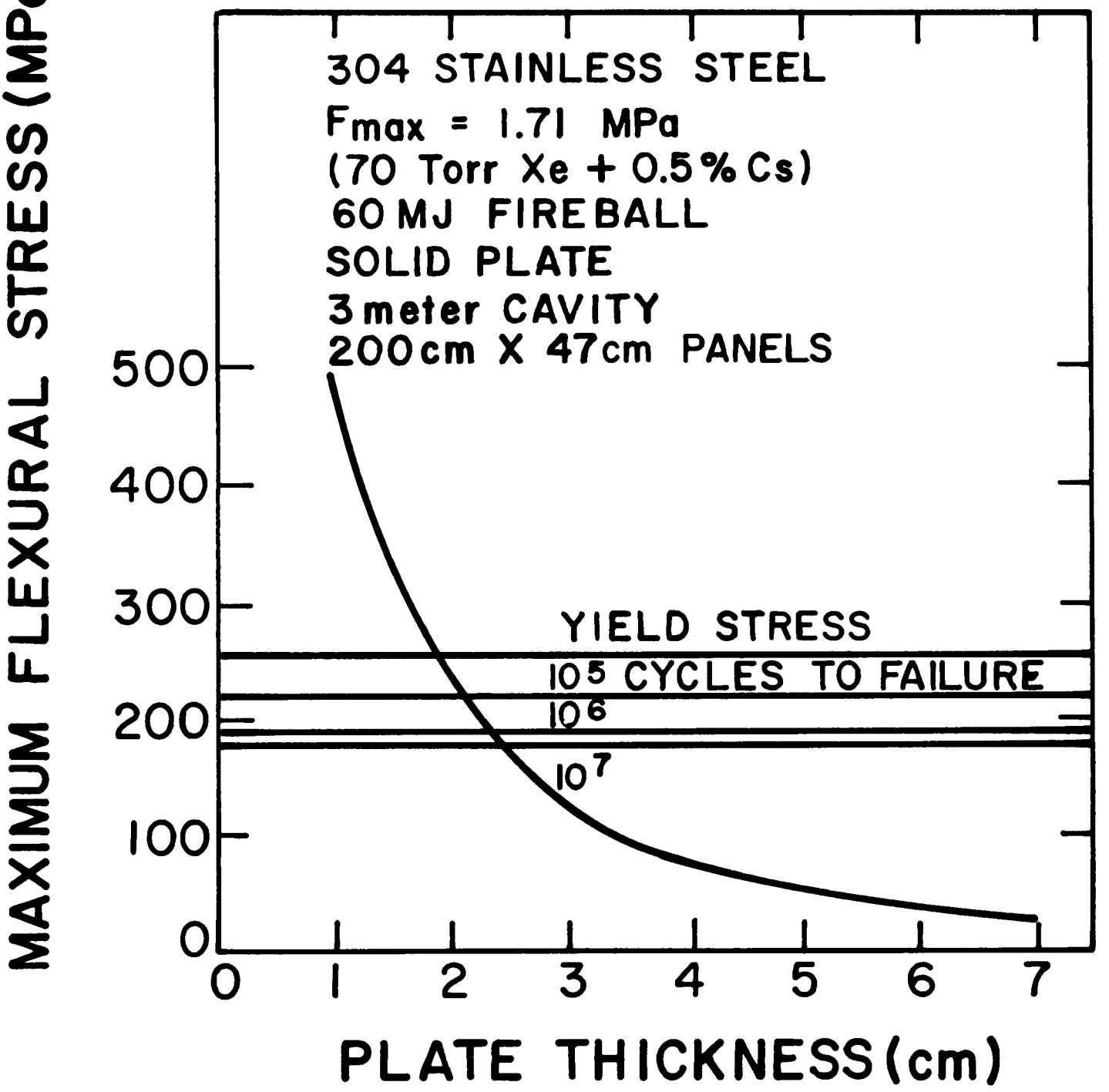

Fig. 7.

Maximum flexural stresses in a plate of HT-9 versus plate thickness for the pressure pulse shown in Fig. 2.

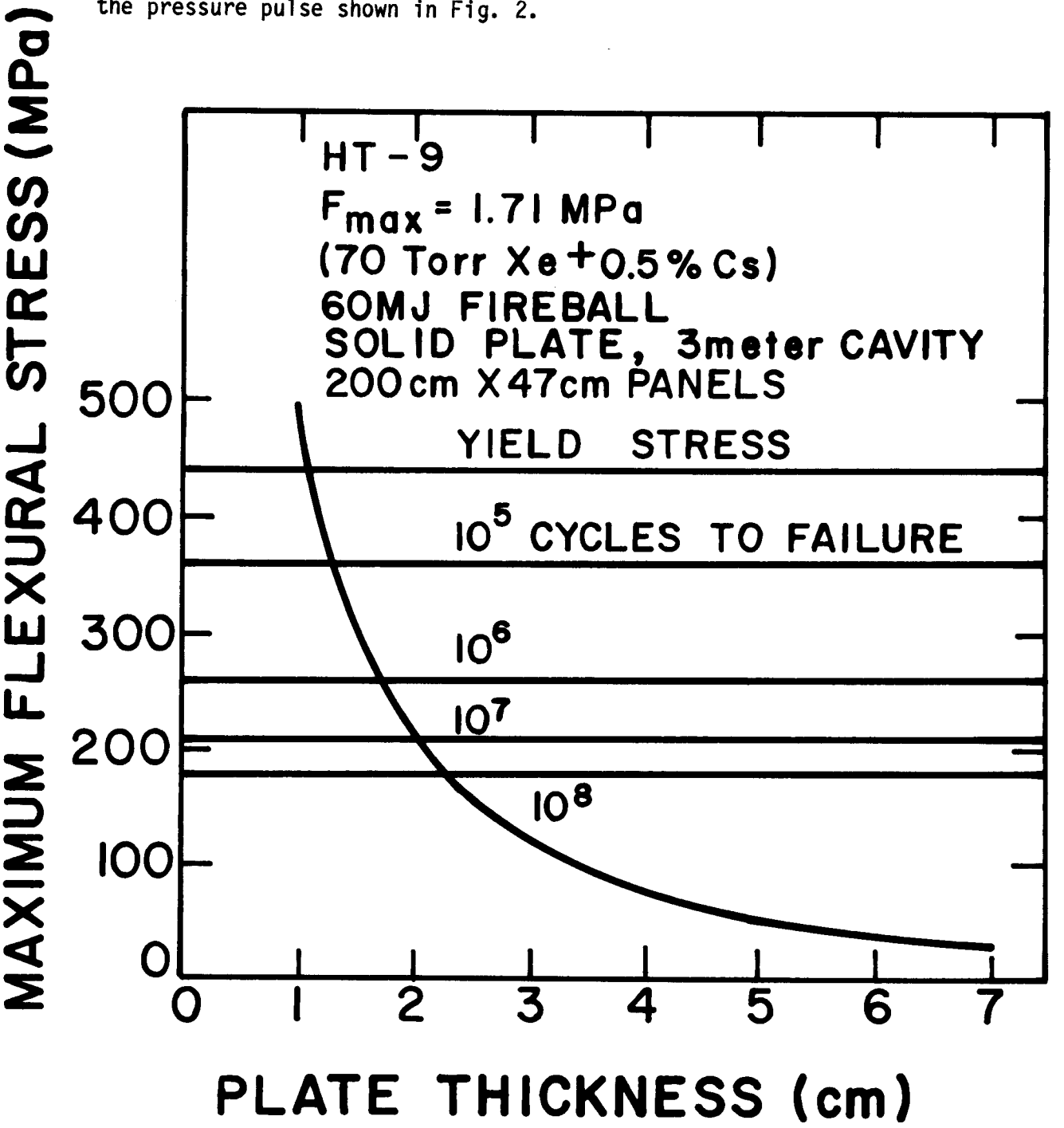

Fig. 8.

Maximum flexural stresses in a plate of Ti-6Al-4V versus plate thickness for the pressure pulse shown in Fig. 2.

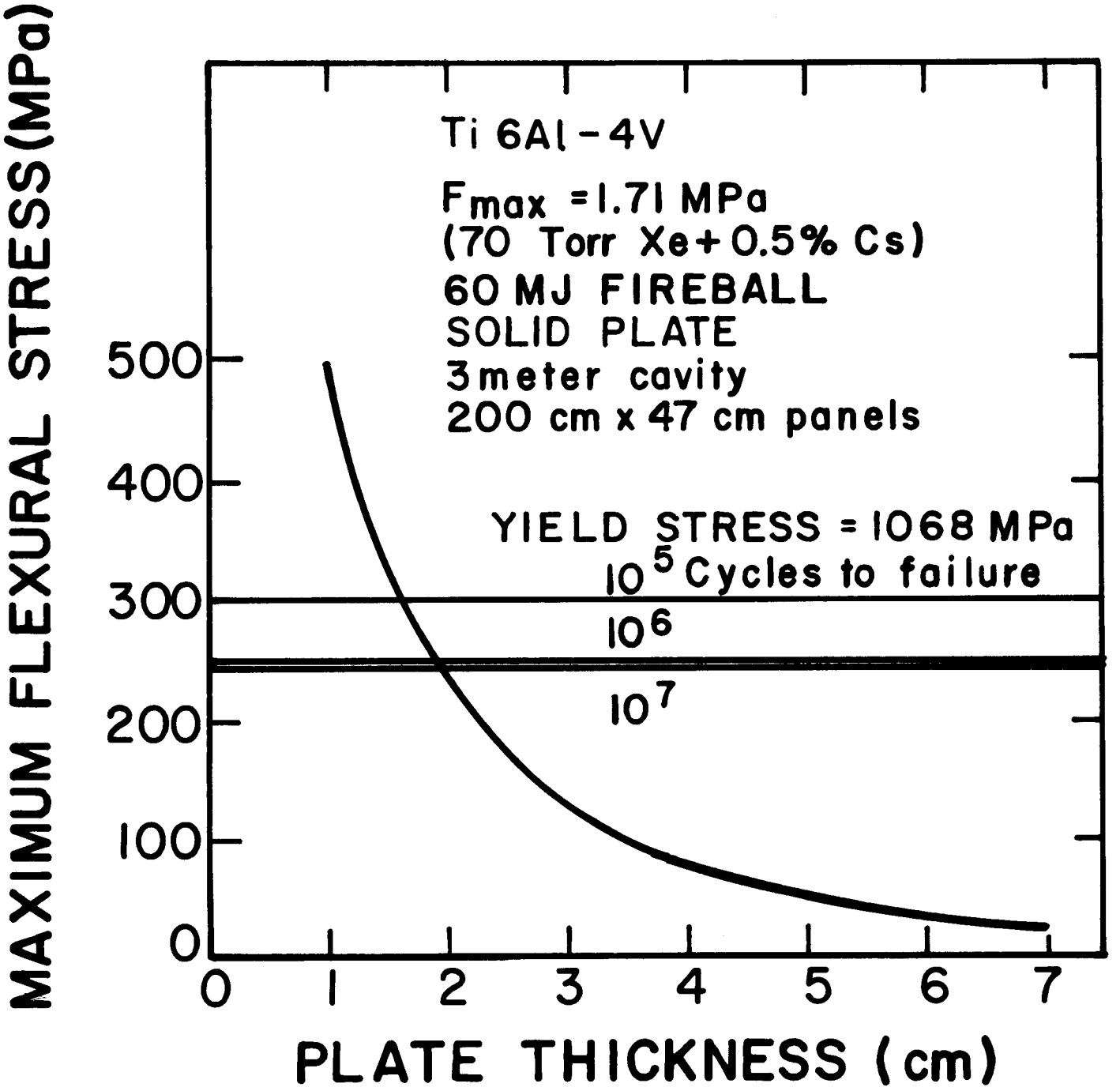

Fig. 9.

Maximum flexural stresses in a plate of Cu-Be C17200 versus plate thickness for the pressure pulse shown in Fig. 2.

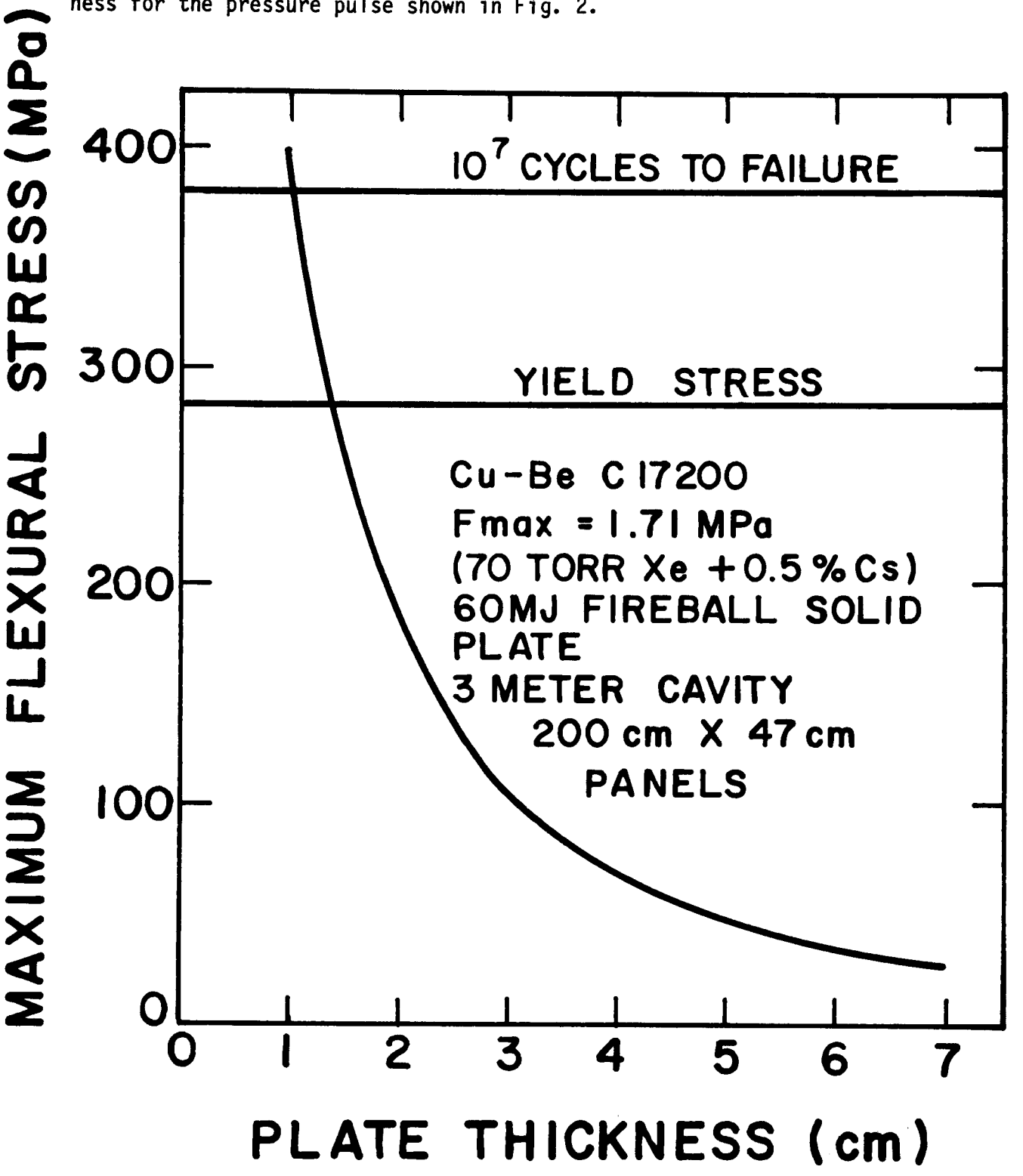

comparable plots for Al 5086 and Cu-Be C17600, but they are very similar to Al 6061 and Cu-Be C17200 and are not shown. Also shown in Figs. 5 through 9 are the stresses corresponding to fatigue failure after a given number of flexures[8] and the tensile yield stresses.

With the results in these figures, the plate thickness required for each material may be determined. The thickness is the maximum of the value corresponding to 10^7 cycles to failure and the value corresponding to the yield stress. Only Cu-Be C17200 and Cu-Be C17600 have their thickness determined by the yield stress. The required thicknesses of all of the materials are given in Table V.

IV. Thermal Response of the First Wall

The second important consideration in first wall design is the thermal response of the wall panels. It is possible that a large fraction of the 60 MJ of non-neutronic target yield may be deposited on the first wall in a fraction of a millisecond. Under such conditions the first wall material may melt or experience large thermal stresses which can cause inelastic deformations or creep. The philosophy used here is to assume the largest possible surface heat flux and analyze the behavior of the innermost layer of the material which undergoes these effects. As long as the effects of heating remain in this layer, e.g., there is no significant growth of cracks, the layer may be treated separately from the remainder of the plate. The load of the shock overpressure is carried by the part of the plate behind the thermally stressed and melted layer and the thickness of the load bearing region is that determined from yield stress and fatigue considerations in Section III.

The heat flux used in the analysis of the thermal response is that which results from a fireball simulation[12] of 60 MJ of non-neutronic target energy

Table V. Thickness Required to Avoid Excessive Flexural Stresses

Material	Thickness (cm)
Al 6061	3.0
Al 5086	3.0
304 SS	2.4
HT-9	2.0
Ti-6Al-4V	1.95
Cu-Be C17200	1.1
Cu-Be C17600	2.15

propagating through a 5 torr xenon gas with a 0.5% impurity of cesium. The heat flux at the first wall of a 3 meter target chamber is shown in Fig. 10. Notice that in this case roughly 90% of the fireball energy is radiated to the first wall in less than a millisecond.

The temperature profile in the first wall is calculated using the heat flux shown in Fig. 10 by using a simple temperature diffusion computer code with constant heat transfer coefficients. An example of this type of calculation for Al 6061 is shown in Fig. 11. The temperature of the first wall is plotted against the distance into the wall for different times. Also shown are the melting temperature of the material, one half of the melting temperature and the temperature causing a 0.1% deformation in the material. A material hotter than one half of the melting temperature may be assumed to creep and any deformation greater than or equal to 0.1% may be taken as inelastic. From plots like Fig. 11, the duration and width of the layer of melted material may be deduced. The duration of the melt layer in Al 6061 is estimated to be 4.7×10^{-4} seconds.

This temperature diffusion code nelgects the heat of fusion and thus overestimates the temperature in the melted layers. A*THERMAL, a more sophisticated temperature diffusion code[13] which includes the effects of heat of fusion has been used to do the same calculation as shown in Fig. 11 and gives the result shown in Fig. 12. Here the surface temperature is plotted against time. Notice that the discontinuity in the heating of the wall surface through the melting temperature is very small, which means that the heat of fusion uses only a small fraction of energy radiated to the wall. Also notice that the film of molten material resolidifies in 4×10^{-4} seconds, which agrees well with 4.7×10^{-4} seconds predicted by the less sophisticated

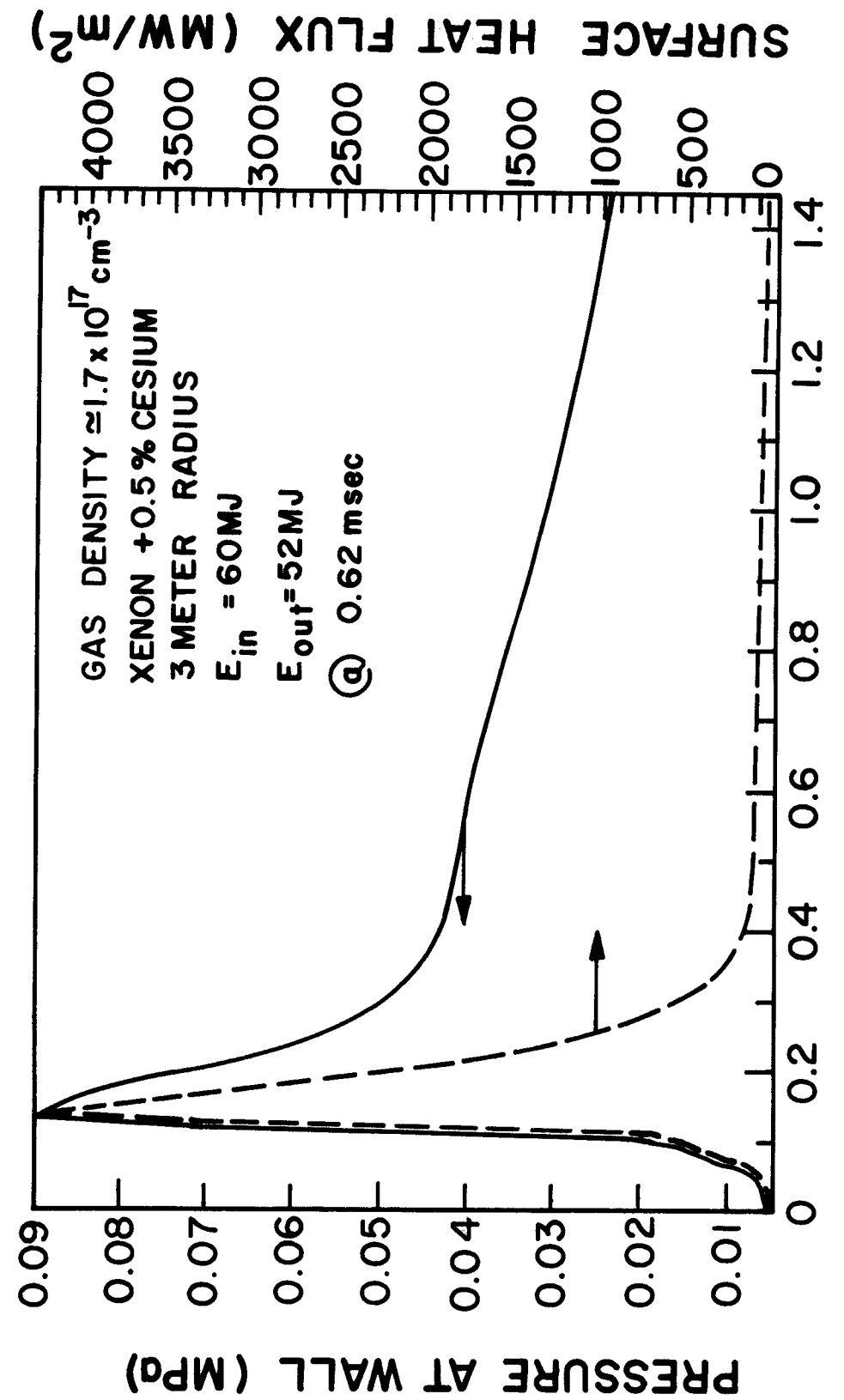

Heat flux and shock overpressure on a 3 meter radius first wall resulting from a 200 MJ microexplosion in a 5 Torr gas of xenon with 0.5% cesium.

Fig. 11

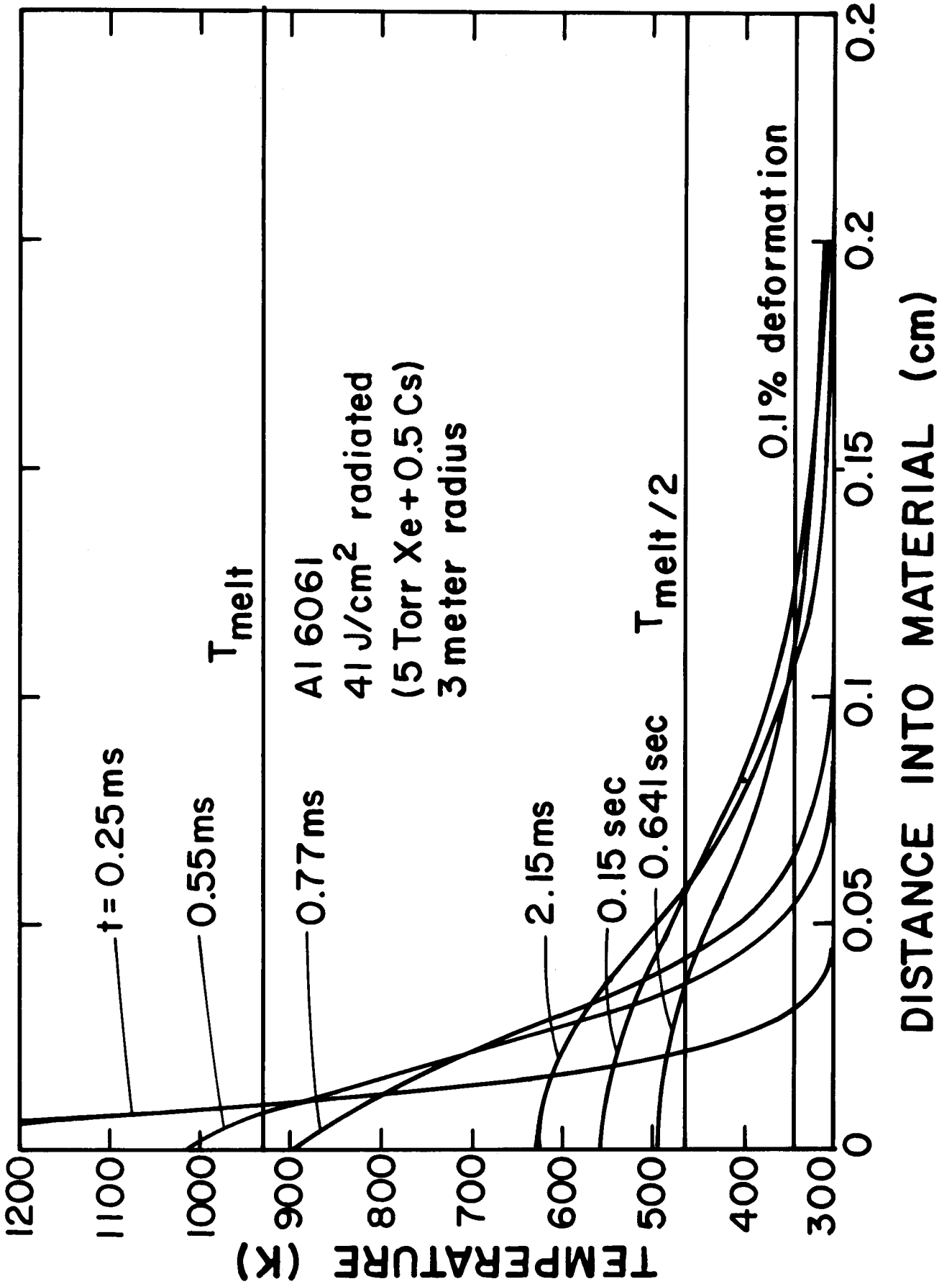

Temperature profiles in an Al 6061 plate versus distance into plate for the heat flux shown in Fig. 10.

Fig. 12

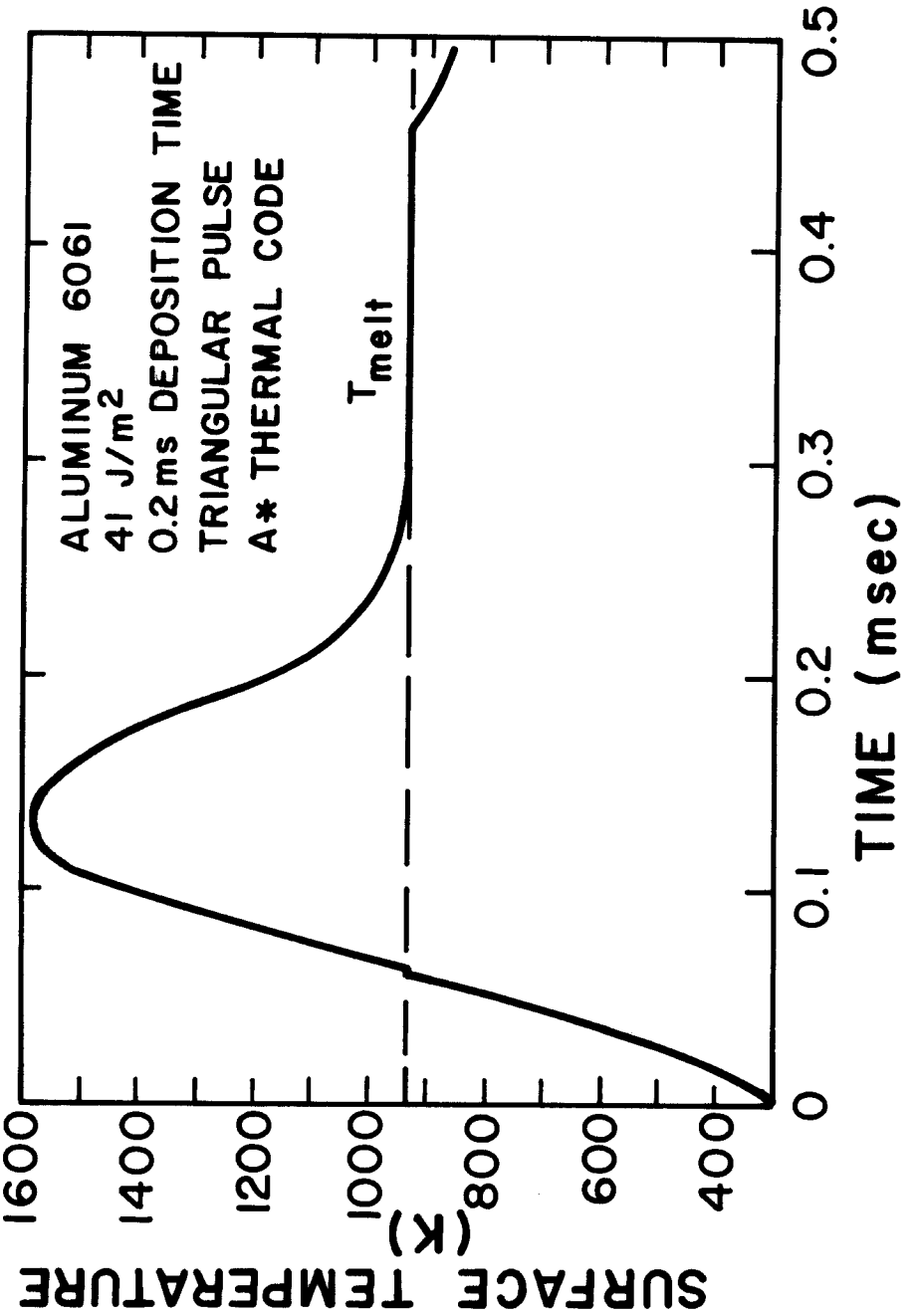

Surface temperature in an Al 6061 plate versus time for the heat flux shown in Fig. 10 as calculated with A*THERMAL.

analysis. This agreement between the two calculations allows the neglect of the heat of fusion in all of the following calculations.

In Figs. 13 through 18 temperature profiles for various times are plotted for Al 5086, 304 stainless steel, HT-9, Ti-6Al-4V, Cu-Be C17200, and Cu-Be C17600, respectively. The calculations leading to these plots have neglected the effects of heat of fusion. The thermal properties of the materials were taken from Table III. It may be noted that the materials with high thermal conductivities, namely the Cu-Be and Al alloys, have low and broad temperature profiles, as one would expect. Conversely, those materials with low thermal conductivities (304 stainless steel, HT-9, and Ti-6Al-4V) have high and narrow temperature profiles. Also shown in these plots are the melting temperatures, one half of that temperature, and the temperature needed for 0.1% deformation.

Using the temperature profiles and the melting temperatures and temperatures for 0.1% deformation shown in Figs. 11 and 13 through 18, the duration and thickness of the layers of melted material and the thicknesses of the inelastically deformed regions can be determined. The purpose of this is to find the thickness of that region which is not able to support the load of the shock overpressure because of the combined effects of melting and thermal stresses. The thicknesses of the layers dedicated to bearing the effects of the thermal pulse are given for each material in Table VI. Also given in Table VI are the thicknesses needed to support the mechanical load and the total thickness for each material. The material which requires the thinnest plate is Cu-Be C17200 because it has a high thermal conductivity, a moderate melting temperature, a moderate Young's modulus and good fatigue resistance. The material which requires the thickest plate is Al 6061 because, even though it has a high thermal conductivity, the melting temperature is low so that it

Fig. 13

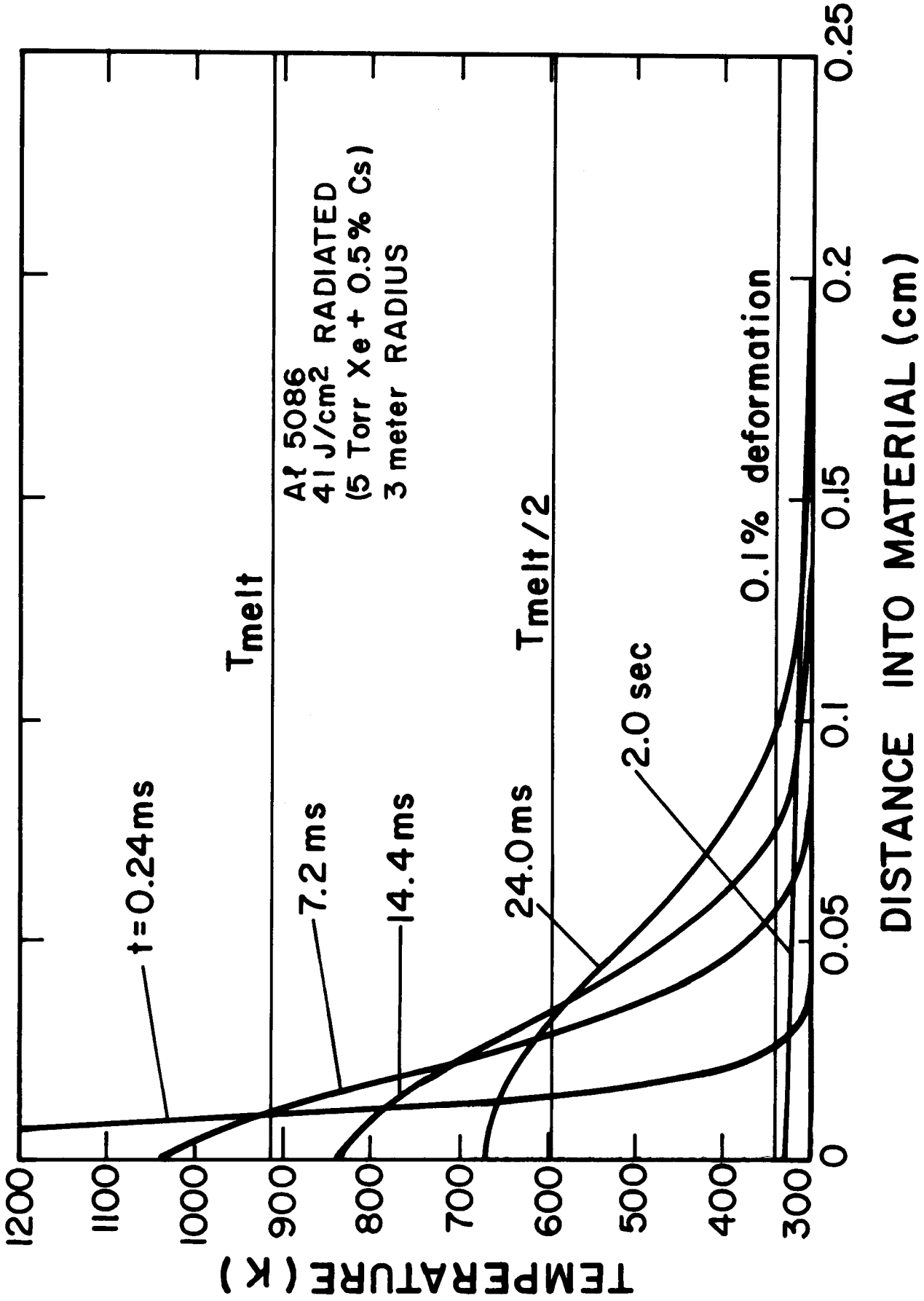

Temperature profiles in an Al 5086 plate versus distance into plate for the heat flux shown in Fig. 10.

Fig. 14

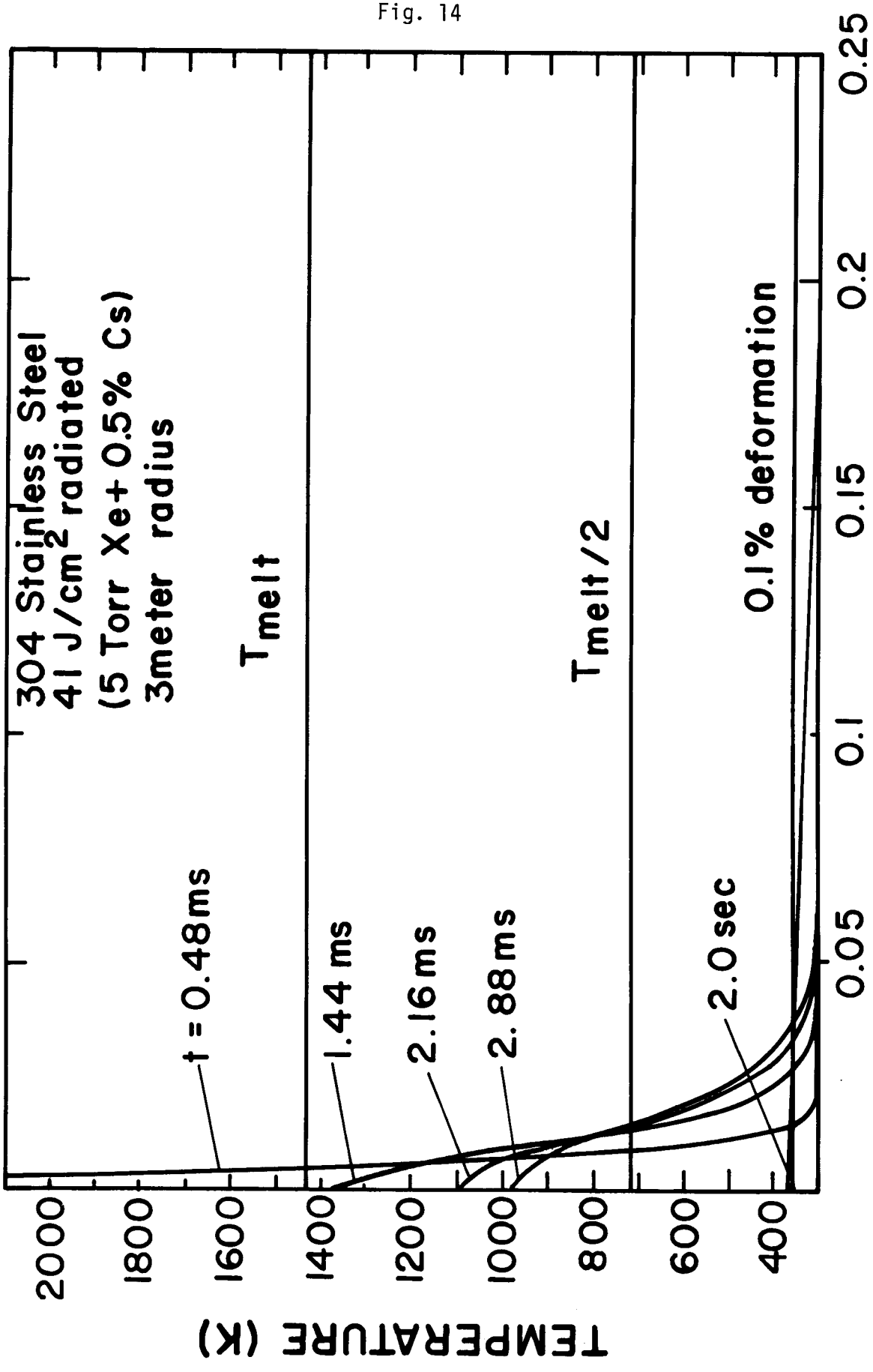

Temperature profiles in a 304 stainless steel plate versus distance into plate for the heat flux shown in Fig. 10.

Fig. 15

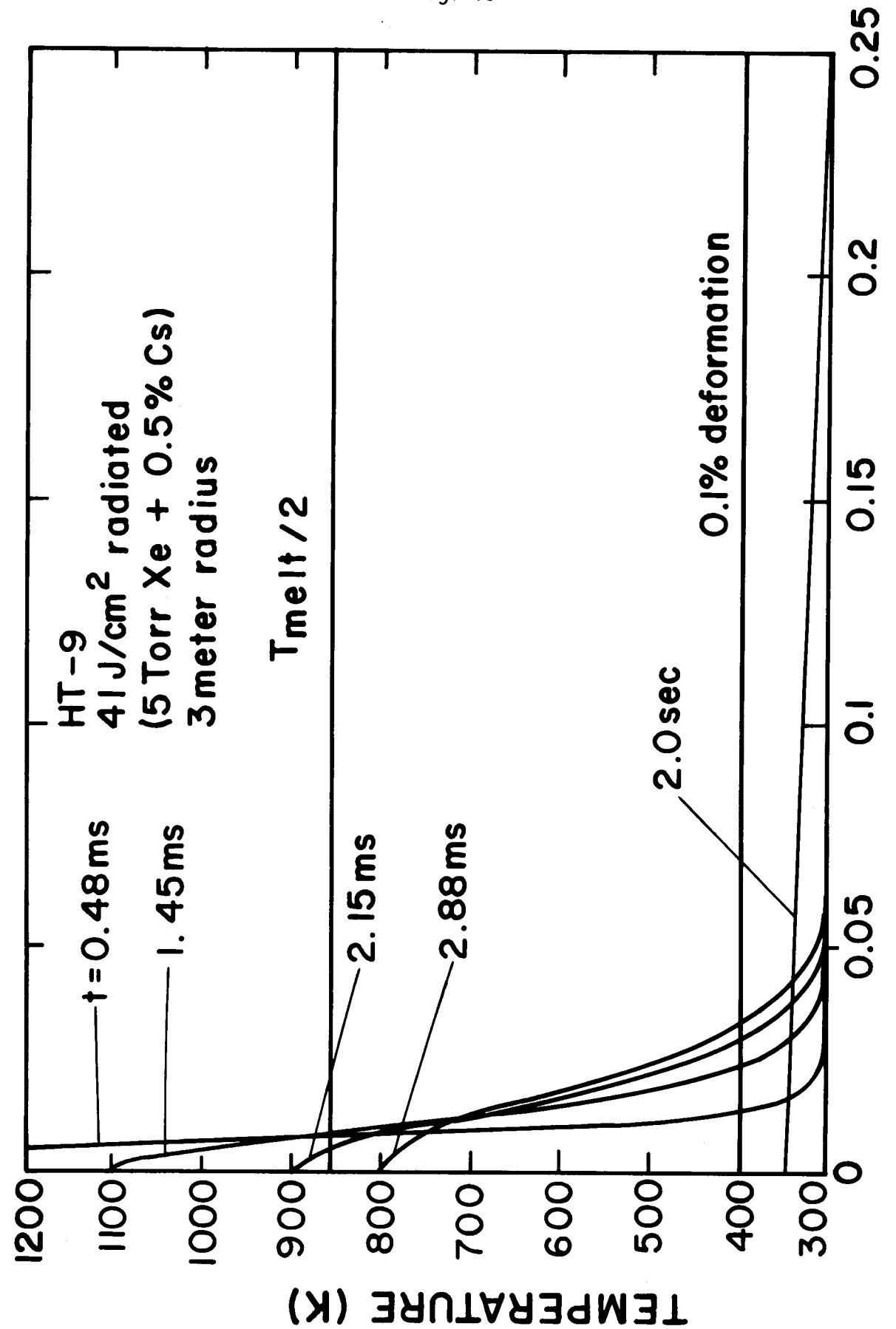

Temperature profiles in a HT-9 plate versus distance into plate for the heat flux shown in Fig. 10.

Fig. 16

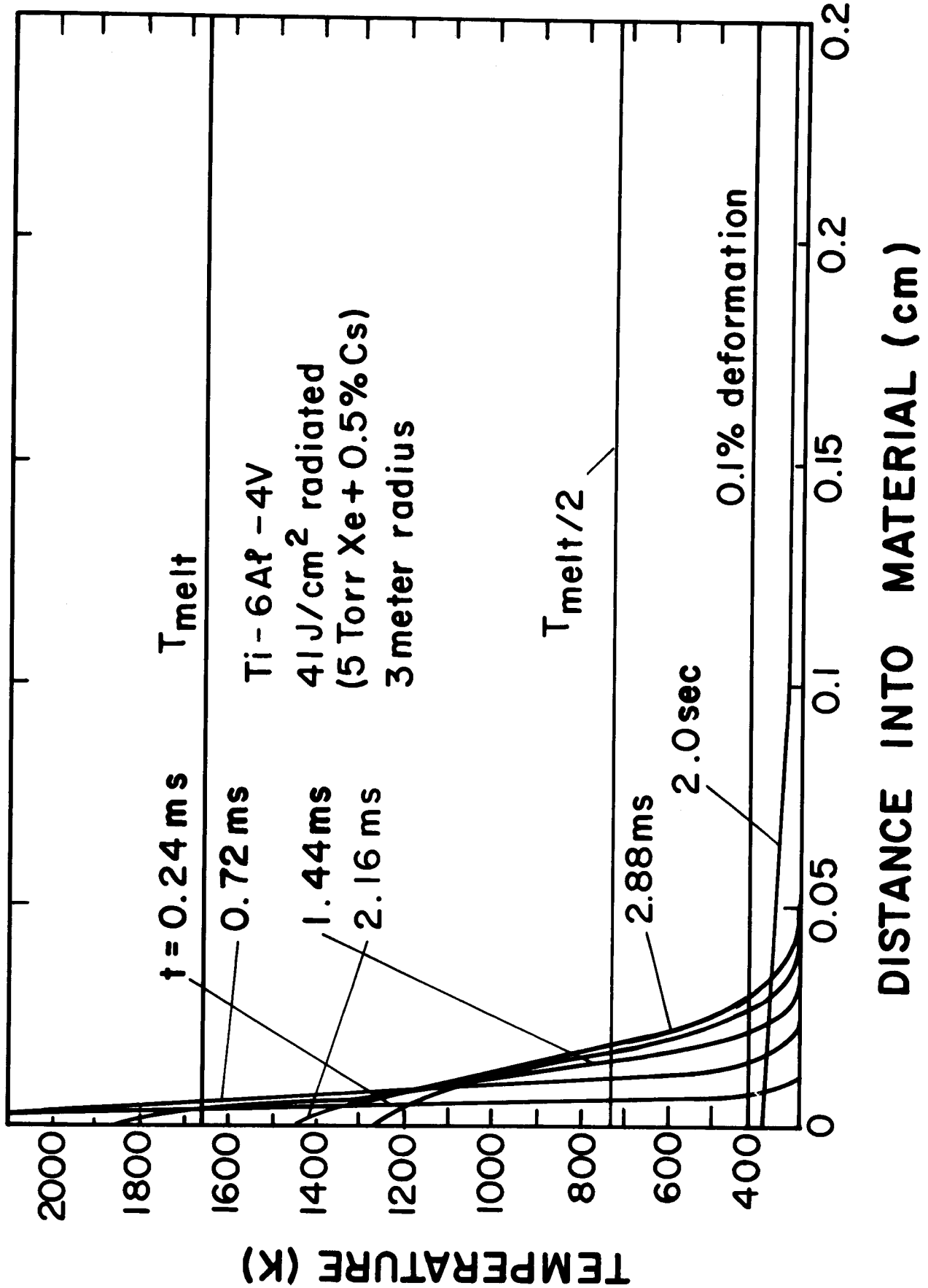

Temperature profiles in a Ti-6Al-4V plate versus distance into plate for the heat flux shown in Fig. 10.

Fig. 17

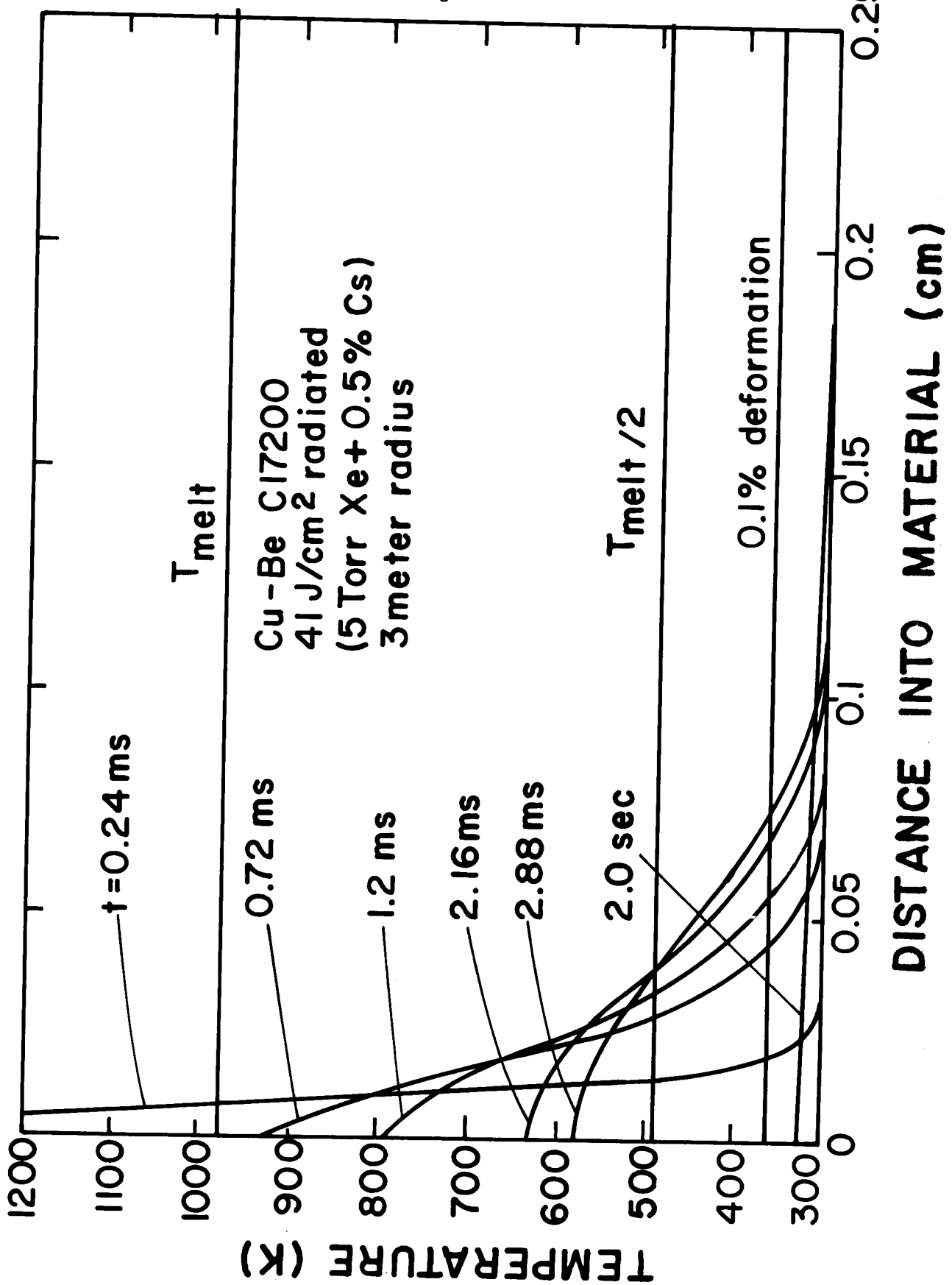

Temperature profiles in a Cu-Be C17200 plate versus distance into plate for the heat flux shown in Fig. 10.

Fig. 18

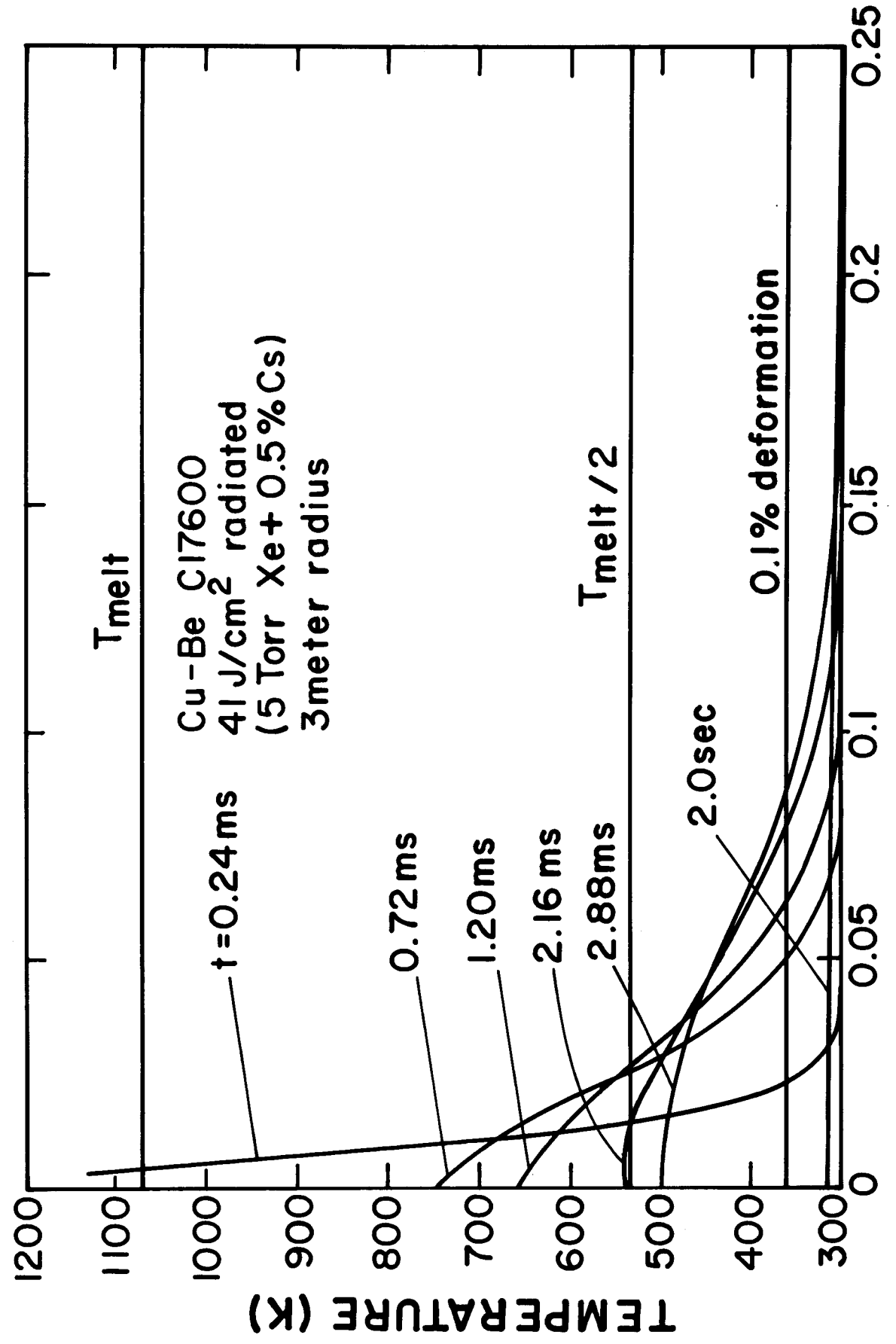

Temperature profiles in a Cu-Be C17600 plate versus distance into plate for the heat flux shown in Fig. 10.

Table VI. First Wall Thermal and Mechanical Response

Material	Melt Layer (cm)	Duration (s)	Deformed Layer (cm)	Fatigue* Width (cm)	Total Plate Thickness (cm)
Al 6061	0.010	4.7×10^{-4}	0.140	3.00	3.140
Al 5086	0.011	4.7×10^{-4}	0.11	3.00	3.11
304 SS	0.0055	2.7×10^{-4}	0.035	2.40	2.44
HT-9	0.0035	7×10^{-4}	0.040	2.0	2.04
Ti-6Al-4V	0.005	2×10^{-3}	0.030	1.95	1.98
Cu-Be C17200	0.007	7×10^{-4}	0.075	1.10	1.16
Cu-Be C17600	0.004	3×10^{-4}	0.086	2.15	2.23

*10^7 cycles or yield stress

has the thickest molten layer. It also has poor fatigue resistance which means that the thickness needed for the mechanical load is large. All materials need thicknesses between 1.16 cm and 3.14 cm, values that are reasonable for construction purposes. In Section V, these plate thicknesses will allow the costs of the materials needed in each case to be determined.

In the above analysis, there are a few assumptions which should be discussed. One such assumption is that cracks generated in the regions undergoing thermal creep will not propagate into the mechanical load bearing regions. This is a reasonable premise because the thickness of the regions where the temperature is between T_{melt} and $T_{melt}/2$ is always small compared with the thickness of the load bearing regions. The crack tips will quickly move into an area where tensile stresses are always small. Another premise is that molten material does not flow before it resolidifies. This is reasonable because the melted layers are always thin, so cohesion with the solid layer is large, the duration of the molten layer is short and the only force parallel to the plane of the plate is gravity. Thus flow of molten material (if any) is not expected to be a problem.

A final point to be made is that the calculations of the temperature profiles predict that 304 stainless steel, HT-9 and Ti-6Al-4V are vaporized to a small degree. The latent heat of vaporization and heat of fusion are neglected so that it is not certain if any vaporization in fact would take place. Also, the heat flux used in these calculations represents the worst case. However, there does remain the possibility that a wall made of one of these materials may be eroded by vaporization.

V. Material Costs

The costs of the materials used in constructing a first wall can be obtained from the wall thicknesses determined in Section IV. The costs of construction are much more difficult to obtain and are not considered here. To a first approximation, the construction costs should be independent of choice of material and should be added to the cost of the materials to find the total cost of the cavity. The costs of the materials themselves are variable, depending on the forms of the materials, the purities needed from radioactivity considerations, etc. The purpose here is not to provide absolute numbers for the material costs but to provide relative costs that will show how the thicknesses of the materials are balanced by the different unit costs of the materials.

The material costs are given in Table VII. The unit costs ($/kg) were obtained from a common source[14] with the exception of HT-9.[15] The masses shown are the total of the 3 meter radius 6 meter high cylindrical cavity, plus the mass of the hemispherical top and bottom. The supporting frame may be assumed to weigh 1.5 times the weight of the wall and the top and bottom, but it is not included in the masses in Table VII.

The cost analysis shows that even though the aluminum walls are the thickest, the material used is the cheapest of all materials considered. Conversely, one of the thinnest walls is made of Ti-6Al-4V but it also has the largest materials cost. In any event, none of these costs appear to be prohibitively large.

VI. Radioactivity

The radioactivity induced in the first wall and supporting structure by 14 MeV fusion neutrons can cause troublesome maintenance and operating

Table VII. First Wall Panel Materials Costs (Unfabricated)

Material	Unit Cost ($/kg)	Mass (kg)	Cost ($)
Al 6061	1.8	1.92×10^4	3.5×10^4
Al 5086	1.8	1.89×10^4	3.4×10^4
304 SS	1.26	4.42×10^4	5.56×10^4
HT-9	18.	3.58×10^4	6.44×10^5
Ti-6Al-4V	27.8	1.98×10^4	5.5×10^5
Cu-Be C17200	8.35	2.16×10^4	1.8×10^5
Cu-Be C17600	8.35	4.72×10^4	4.0×10^5

problems for the Target Development Facility. We anticipate that the radioactive inventory will not pose a disposal problem so we have concentrated on the resultant dose from this radioactive structure. We assume that there are ten full yield 200 MJ shots per day. This represents an average fusion power level of 23 kW. We assume that 70% of the energy is in neutrons. Hence, the neutron power is 16 kW. At such low power levels, in comparison to our fusion reactor designs for instance, we would expect that there may be non-saturation effects in the decay chains. For this reason we have computed the dose for one week and for one year of operating time at 16 kW. These calculations have thus far been done for three of our candidate wall materials: Al 6061, HT-9, and 304 stainless steel. The isotopic compositions of these materials are given in Table VIII. The radiation doses experienced at the surface of the first wall and from the operating floor, 8 meters away, are given in Tables IX and X. In Table IX we show the dose at these two locations as a function of time after shutdown after operating for one year. We see that for Al 6061, we could enter the target chamber at one week after shutdown without experiencing excessive doses. For the ferritic and stainless steels we would see a substantial dose at the first wall even after one week. It is interesting to note that the Al 6061 is much hotter at shutdown than the steels, but it decays much more quickly. If remote handling were acceptable then the steels would allow manipulation from the operating floor while remaining within tolerable radiation levels. This scenario of course assumes that access to the target chamber will be very infrequent.

In Table X we give the results of calculations assuming only one week of operation before shutdown. Again, the Al 6061 is very hot at first and then quickly decays. The steels reach nearly the same dose levels at shutdown, but

Table VIII. Isotopic Composition of 304 SS, HT-9, and Al 6061 (cm^{-3})

304 SS

Si-28	7.3×10^{20}	Si-29	3.72×10^{19}	Si-30	2.38×19^{19}
Cr-50	6.94×10^{20}	Cr-52	1.35×10^{22}	Cr-53	1.54×10^{21}
Cr-54	3.83×10^{20}	Mn-55	1.01×10^{21}	Fe-54	3.48×10^{21}
Fe-56	5.48×10^{22}	Fe-57	1.31×19^{21}	Fe-58	1.97×10^{20}
Ni-58	5.09×10^{21}	Ni-60	1.97×10^{21}	Ni-61	8.92×10^{19}
Ni-62	2.74×10^{20}	Ni-64	8.10×10^{19}	Cu-63	1.03×10^{20}
Cu-64	4.60×10^{19}	Mo-92	2.58×10^{19}	Mo-94	1.47×10^{19}
Mo-95	2.56×10^{19}	Mo-96	2.69×10^{19}	Mo-97	1.54×10^{19}
Mo-98	3.88×10^{19}	Mo-100	1.57×10^{19}		

HT-9

Si-28	3.9×10^{20}	Si-30	1.2×10^{19}	V-50	2.75×10^{20}
Cr-50	4.47×10^{20}	Cr-52	8.7×10^{21}	Cr-53	9.91×10^{20}
Cr-54	2.47×10^{20}	Mn-55	4.27×10^{20}	Fe-54	4.17×10^{21}
Fe-56	6.56×10^{22}	Fe-57	1.57×10^{21}	Fe-58	2.36×10^{20}
Ni-58	2.71×10^{20}	Ni-60	1.04×10^{20}	Ni-62	1.46×10^{19}
Ni-64	4.3×10^{17}	Mo-92	7.75×10^{19}	Mo-95	7.7×10^{19}
Mo-96	8.1×10^{19}	Mo-97	4.6×10^{19}	Mo-98	1.16×10^{20}
Mo-100	4.7×10^{19}	W-174	2.0×10^{17}	W-182	3.4×10^{19}
W-183	1.8×10^{19}	W-184	3.9×10^{19}	W-186	3.6×10^{19}

Al 6061

Mg-24	4.74×10^{20}	Mg-25	6.11×10^{19}	Mg-26	6.73×10^{19}
Al-27	5.82×10^{22}	Si-28	3.20×10^{20}	Si-29	1.63×10^{19}
Si-30	1.07×10^{19}	Cr-50	4.04×10^{18}	Cr-52	7.86×10^{19}
Cr-53	8.96×10^{18}	Cr-54	2.23×10^{18}	Mn-55	4.44×10^{19}
Fe-54	1.19×10^{19}	Fe-56	1.87×10^{20}	Fe-57	4.46×10^{18}
Fe-58	6.73×10^{17}	Cu-63	5.30×10^{19}	Cu-65	2.37×10^{19}

Table IX. Dose Calculations for LIB-TDF

One Year Operating Time @ 16 kW

Time After Shutdown	Dose At First Wall (mr/hr)	Dose At Operating Floor (mr/hr)
	Al 6061	
0	2.1×10^3	230
1d	2.6×10^2	28
1w	1.65	0.18
	HT-9	
0	489	55
1d	114	13
1w	101	11
	SS 304	
0	481	54
1d	109	12
1w	105	12

Table X. Dose Calculations for LIB-TDF

One Week Operating Time @ 16 kW

Time After Shutdown	Dose At First Wall (mr/hr)	Dose At Operating Floor (mr/hr)
	Al 6061	
0	2.1×10^3	2.3×10^2
1d	264.	28.
1w	0.4	4×10^{-2}
	HT-9	
0	369.	42.8
1d	13.9	1.56
1w	2.58	0.23
	SS 304	
0	373.	43.3
1d	5.8	0.66
1w	3.6	0.42

their longer-lived radionuclides have not saturated, hence the dose at one week after shutdown is tolerable. However, this dose will build up over time so that in one year it will be nearly the same as in the previous scenario.

We see that the radiation fields associated with an aluminum wall and structure are initially more intense than for steel. But they decay much more quickly so that one week after shutdown, the dose is low enough to allow hands-on access to the target chamber. This is not the case for the steels. However, remote access from the operating floor is possible after one week for the steel structure.

An important element of this analysis that has not been addressed is the problem of radioactive target debris and tritium. The target ablator and pusher will experience very intense neutron fields which will lead to some radioactive inventory. The mass transport of the material within the gas filled target chamber is a complex problem that has not been addressed in this study. Although tritium is a benign radioactive isotope, it will be present in copious amounts. Hence any adsorption or absorption of tritium in the target chamber will lead to radioactive hazards that have not been addressed.

From the analysis that has been done thus far, the best choice from a radioactivity standpoint is aluminum. It should be mentioned that high purity aluminum is available if dose levels from impurities pose a serious problem. However, from our current results we conclude that this additional expense is not necessary.

VII. Conclusions

The choice of first wall material has been investigated for the TDF. Mechanical and thermal properties have been accumulated for the materials considered. Mechanical responses have been predicted for the largest credible

shock overpressure and thermal responses have been determined for the largest heat flux on the first wall. Induced radioactivity has been calculated for walls made of some of the materials. Required thicknesses and material costs are finally found for the materials.

It has been found that Al 6061 is a good choice of material for the TDF first wall. Calculations show that one week after shutdown, the radioactivity is low enough for hands-on maintenance. Cost estimates also show that the aluminum alloys are the cheapest of those materials considered. The thicknesses needed for these alloys are reasonable for construction. The major problem with aluminum is its incompatibility with Na and Cs. Recall that these impurities in the cavity gas are present to enhance channel breakdown by laser beams. This leads us to suggest that other cavity gas candidates be investigated for the TDF. With this qualification Al 6061 is suggested for serious consideration as the first wall material.

Acknowledgment

This work was supported by Sandia National Laboratories under contract DE-AS08-81DP40161.

References

1. Lawrence Livermore Laboratory Laser Fusion Annual Report - 1978, UCRL-50021-78.

2. R.W. Conn et al., "SOLASE - A Conceptual Laser Fusion Reactor Design," University of Wisconsin Fusion Engineering Program Report UWFDM-220 (Dec. 1977).

3. E.W. Sucov, "Inertial Confinement Fusion Central Station Electrical Power Generation Plant," DOE/DP/40086-1 (Feb. 1981).

4. B. Badger et al., "HIBALL - A Conceptual Heavy Ion Beam Driven Fusion Reactor Study," University of Wisconsin Fusion Engineering Program Preliminary Report UWFDM-450/KfK-3202 (June 1981).

5. D.L. Cook et al., "Light Ion Driven Inertial Fusion Reactor Concepts," Proc. of the 4th Topical Mtg. on the Technology of Controlled Nuclear Fusion, King of Prussia, PA, Oct. 14-17, 1980, pp. 1386-1394.

6. G.A. Moses and R.R. Peterson, "FIRE - A Computer Code to Simulate Cavity Gas Response to Inertial Confinement Target Explosions," University of Wisconsin Fusion Engineering Program Report UWFDM-336 (Jan. 1980); also, T.J. McCarville, R.R. Peterson, and G.A. Moses, "Improvements in the FIRE Code for Simulating the Response of a Cavity Gas to Inertial Confinement Fusion Target Explosions," University of Wisconsin Fusion Engineering Program Report UWFDM-407 (June 1981).

7. "Aerospace Structural Metals Handbook," Mechanical Properties Data Center, Belfour Stalen, Inc., Traverse City, MI, (1975, 1981).

8. "Metals Handbook," 9th Ed., American Society for Metals, Metals Park, OH, (1979).

9. "Structural Alloys Handbook," Battelle Columbus Laboratories, Columbus, OH, (1981).

10. C.C. Baker et al., "STARFIRE - A Commercial Tokamak Fusion Power Plant Study," Argonne National Laboratory ANL/FPP-80-1 (1980).

11. E.G. Lovell, R.R. Peterson, R.L. Engelstad, and G.A. Moses, "Transient Elastic Stresses in ICF Reactor First Wall Structural Systems," University of Wisconsin Fusion Engineering Program Report UWFDM-421 (Aug. 1981), presented at the 2nd Topical Meeting on Fusion Reactor Materials, 9-12 August 1981, Seattle, WA.

12. R.R. Peterson, K.J. Lee, and G.A. Moses, "Low Density Cavity Gas Fireball Dynamics in the Light Ion Beam Target Development Facility," University of Wisconsin Fusion Engineering Program Report UWFDM-442 (Oct. 1981), presented at 9th Symposium of Engineering Problems of Fusion Research, 26-29 October 1981, Chicago, IL.

13. A.M. Hassanein and G.L. Kulcinski, "A*THERMAL Code Description," University of Wisconsin Fusion Engineering Program Report (in preparation).

14. Materials in Design Engineering, Materials Selector Issue.

15. "Fusion Reactor Design Studies: Standard Cost Estimating Rules," Battelle Pacific Northwest Laboratories PNL-2987.